A&A 570, A84 (2014)
DOI: 10.1051/0004-6361/201423970

Astronomy & Astrophysics

Dynamics of a multi-thermal loop in the solar corona*

G. Nisticò[1], S. Anfinogentov[2], and V. M. Nakariakov[1,3,4]

[1] Centre for Fusion, Space and Astrophysics, Department of Physics, University of Warwick, Coventry CV4 7AL, UK
e-mail: g.nistico@warwick.ac.uk
[2] Institute of Solar-Terrestrial Physics, Russian Academy of Science, Siberian Branch, 126a Lermontov st., 664033 Irkutsk, Russia
e-mail: anfinogentov@iszf.irk.ru
[3] Central Astronomical Observatory at Pulkovo of the Russian Academy of Sciences, 196140 St. Petersburg, Russia
[4] School of Space Research, Kyung Hee University, Yongin, 446-701 Gyeonggi, Korea

Received 9 April 2014 / Accepted 2 July 2014

ABSTRACT

Context. We present an observation of a long-living multi-thermal coronal loop, visible in different extreme ultra-violet wavebands of SDO/AIA in a quiet-Sun region close to the western solar limb.
Aims. Analysis of persistent kink displacements of the loop seen in different bandpasses that correspond to different temperatures of the plasma allows sub-resolution structuring of the loop to be revealed.
Methods. A vertically oriented slit is taken at the loop top, and time-distance maps are made from it. Loop displacements in time-distance maps are automatically tracked with the Gaussian fitting technique and fitted with a sinusoidal function that is "guessed". Wavelet transforms are further used in order to quantify the periodicity variation in time of the kink oscillations.
Results. The loop strands are found to oscillate with the periods ranging between 3 and 15 min. The oscillations are observed in intermittent regime with temporal changes in the period and amplitude. The oscillations are different at three analysed wavelengths.
Conclusions. This finding suggests that the loop-like threads seen at different wavelengths are not co-spatial, hence that the loop consists of several multi-thermal strands. The detected irregularity of the oscillations can be associated with a stochastic driver acting at the footpoints of the loop.

Key words. Sun: corona – Sun: oscillations – methods: observational

1. Introduction

Observations of the Sun at extreme ultra-violet (EUV) and X-ray wavelengths have shown that the solar corona is structured in the form of 1D curvilinear features that resemble closed loops in active regions, which indicate the presence of strong magnetic fields in the solar corona. These loops act as waveguides for magnetohydrodynamic (MHD) waves. A theory of the propagation of MHD waves in a plasma cylinder has been formulated in seminal works of Zajtsev & Stepanov (1975), Roberts (1981), Roberts et al. (1984), and Edwin & Roberts (1983), distinguishing between several different kinds of fast magnetoacoustic modes. Kink modes are transverse displacements of the loop axis and were first observed with the Transition Region And Coronal Explorer (TRACE) mission (Aschwanden et al. 1999; Nakariakov et al. 1999). Space missions, such as the Solar TErrestrial RElations Observatory (STEREO) and Hinode, have permitted intensive studies of kink oscillations not only in coronal loops but also in prominence fibrils (e.g. Arregui et al. 2012), hot jets (Cirtain et al. 2007; Vasheghani Farahani et al. 2009), and post flare loops arcades (Verwichte et al. 2005). The fundamental mode, i.e. oscillations with nodes at the footpoints and an anti-node at the loop apex, polarised horizontally is mainly observed, but there is evidence of higher harmonics (Verwichte et al. 2004; De Moortel & Brady 2007) and vertically polarised oscillations (Wang & Solanki 2004; White et al. 2012). After being triggered by an impulsive event like a flare or a coronal mass ejection (CME), kink oscillations of coronal loops experience strong damping. Typically, the oscillations only last for three or four periods. Theoretical explanations of this damping have been addressed in terms of "resonant absorption", i.e. conversion of the kink mode to a localised and hence invisible torsional Alfvén mode (Ruderman & Roberts 2002; Goossens et al. 2002, 2012).

Nowadays, the Solar Dynamics Observatory (SDO) space mission allows us to significantly improve our view of the Sun (Lemen et al. 2012). Thanks to the Atmospheric Imaging Assembly (SDO/AIA), which is an array of four telescopes with eight different filters that observe the solar corona at the highest temporal and spatial resolution possible today, a new regime of kink oscillations of coronal loops has been found. Recently Nisticò et al. (2013a) and Anfinogentov et al. (2013) have detected "decay-less" kink oscillations. In this regime the oscillations do not experience damping. Moreover, these oscillations appear without any association to flares or CMEs. A signature of persistent kink oscillations has also been found in Wang et al. (2012), who describe observations of the growing kink oscillations of a coronal loop. The mechanism able to sustain the decay-less regime against the natural damping of kink waves is still unknown. There is also a need to quantify the energy input that supports this mechanism. Thus, this new regime requires a detailed observational study that would provide us with some hints to its understanding and interpretation.

In this paper, we analyse an example of irregular kink displacements of a multi-thermal coronal loop, observed in a quiet-Sun region simultaneously at three EUV wavelengths with SDO/AIA.

* A movie associated to Fig. 1 is available in electronic form at http://www.aanda.org

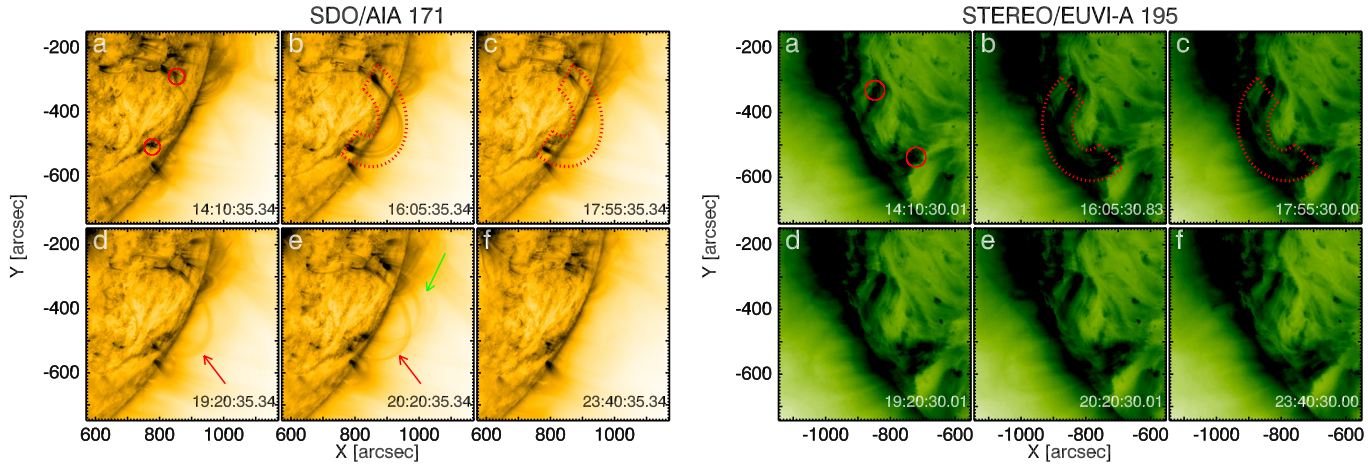

Fig. 1. Snapshots of the multi-thermal loop observed with SDO/AIA at 171 Å (*left*) and STEREO/EUVI-A at 195 Å (*right*). The circles mark the loop footpoints, whilst the dotted region encloses the loop in both views. The red arrow in the *left panels* mark the position of the loop during its evolution and the green one that of a transient loop in AIA. The movie showing the temporal evolution as seen in the 171 Å channel of AIA is available in the online edition.

2. Observations

2.1. The multi-thermal loop

The coronal loop appeared on the south-western limb of the Sun in the field-of-view (FOV) of SDO/AIA on 21 January 2013 and was observed for almost ten hours. The loop had approximately a semi-circular shape and was not associated with any active region. Figure 1 shows a sequence of images demonstrating the temporal evolution of this loop at 171 Å observed with SDO/AIA and at 195 Å with STEREO/EUVI-A.

The loop starts to light up at 171 Å around 14:10 UT (panel a of Fig. 1-left), and initially appears as a very thin semi-circular bright strip. Progressively, several rims appear above the previous one, and the intensity increases. The loop footpoints become very bright, resembling "flaring" (panel b). During the observation, several distinct loop bundles appear, experiencing some transverse displacements and intensity variation. The intensity variations can perhaps be attributed to the line-of-sight integration effect (Cooper et al. 2003). Also the external bundles are brighter than the internal ones, probably from the same line-integration effect since the external bundles may have a bigger column depth along the line-of-sight (panels c, d). At 20:20 UT, another loop appears behind, showing almost the same geometrical shape (panel e). After 23:40 UT, the intensity progressively drops down and the loop disappears. A movie showing the entire evolution of the loop (10 h, starting at 14:00 UT) in the same FOV as Fig. 1 (left) at 171 Å, with a cadence of 1 min, is provided in the online edition.

The same region is visible from the EUV Imager (EUVI) of STEREO-A, showing another perspective of the loop, but the lower spatial and temporal resolution (1.6 arcsec, and 5 min at 195 Å) does not allow capturing the same details. The right-hand panels of Fig. 1 show a sequence of the same region at 195 Å at the same time steps as in Fig. 1 (left). It is possible to see the footpoints where the loop bundles are diverging from (panel a), but it is difficult to track them because of the low signal. The loop is also visible in other EUV bands with SDO/AIA, as seen in the top panels of Fig. 2.

The detection of the loop in the other wavelengths could indicate that it is formed of multi-thermal elementary strands. What is possible to infer is that the footpoints are seen very well at

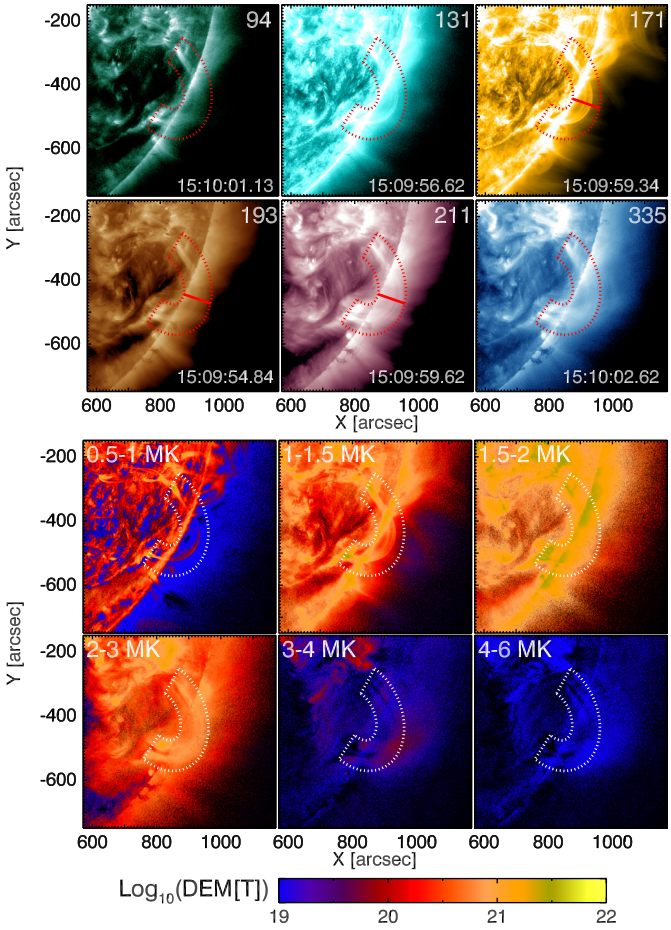

Fig. 2. *Top*: loop at six EUV wavebands of SDO/AIA. *From the left* we have 94, 131, 171 Å (*top row*) and 193, 211, 335 Å (*bottom row*). *Bottom*: DEM maps of the studied region at different temperature ranges. In both panels, the loop is enclosed in a dotted region. The continuous line located at the loop top at 171, 193, and 211 Å marks the position of the slit.

hot temperatures (94, 131, 335 Å), whereas the loop body is more contrasted at "lower" temperatures (171, 193, 211 Å). It is not possible to immediately quantify the temperature of the

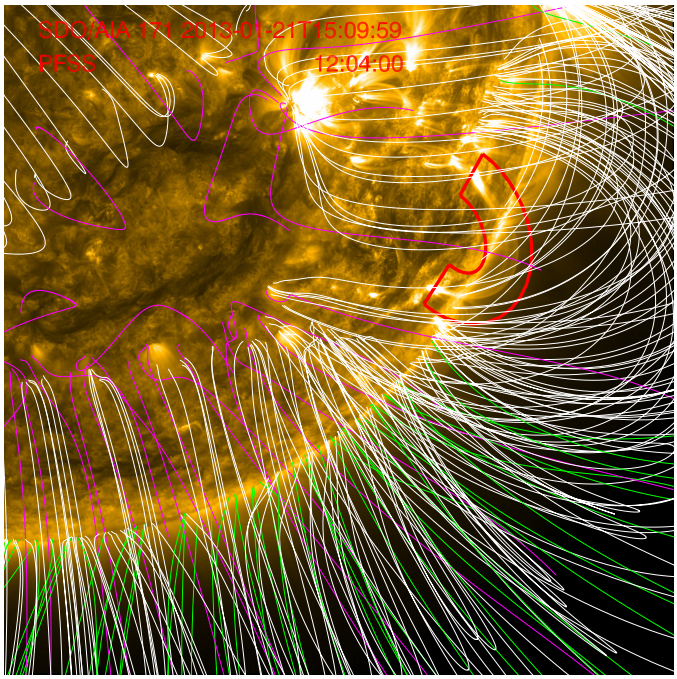

Fig. 3. SDO/AIA image at 171 Å at about 15:10 UT with PFSS extrapolated magnetic field lines over-plotted. The PFSS model refers to about 3 h before the AIA image. The closed magnetic field lines are marked in white, while the open magnetic field lines of positive polarity are in green and negative in purple.

loop or strands, because of the broad-band response in temperature of the AIA filters (for more details see Del Zanna 2013). The regularised inversion technique of Hannah & Kontar (2012) provides a method for getting differential emission measures (DEMs) from AIA data[1]. We applied this technique to obtain DEM maps at several temperature intervals, ranging between 0.5–8 MK (Fig. 2-bottom panel), avoiding any formal discussion on the validity of the method. We simply show that the loop is apparently filled with low-temperature plasma (0.5–1.5 MK) and, as temperatures increase, it becomes "fuzzier". The latter property has been fully studied in Guarrasi et al. (2010).

The overall structure of the loop appears as an "ensemble" of many diverging strands, probably organised in larger bundles, which share the same footpoints. The loop shape reflects the magnetic structure that can be inferred from extrapolation models as the potential field source surface (PFSS), where the magnetic field lines extrapolated from magnetograms are over-plotted on the AIA 171 image (Fig. 3).

2.2. 3D reconstruction

The geometry of the multi-thermal loop was reconstructed in three-dimensional (3D) space by using the principal component analysis (PCA). The details of the technique can be found in Nisticò et al. (2013b). Briefly, it provides an alternative method of fitting a reasonable number of 3D points that sample the loop shape. It mainly consists of finding the typical eigenvalues and the corresponding eigenvectors of the covariance matrix of the 3D points, which will define a set of three axes denoting a new reference frame related to the loop centre, as the normal to the loop plane, the major, and the minor axis of the ellipse that fits the loop. Other parameters, such as the inclination and azimuth angles, are retrieved geometrically from the orientation of this reference frame with respect to the standard solar coordinate system.

The loop has almost a circular shape, since the minor and major radii, as deduced from the 3D reconstruction, are almost comparable, 0.107 and 0.136 $R_\odot$, respectively (see Table 1 of Nisticò et al. 2013b). The loop is almost perpendicular to the solar surface since the estimated inclination is close to 0 deg (measured with respect to the radial direction out of the Sun), and it is mainly oriented along the north-south solar direction since the azimuth angle is about 73 deg. From the AIA perspective, we can therefore say the loop is almost perpendicular to the line-of-sight, since the loop centre is located at heliographic coordinates of (69.23, –25.88) deg, about 20 deg from the west solar limb. The loop shape has been reconstructed at about 14:25 UT and does not seem to undergo significant changes during the time evolution of ten hours, except the local intensity variation of the loop bundles, small transverse motions around the equilibrium, and the solar rotation effects.

2.3. Data overview

To study transverse displacements of the loop, we downloaded FITS files at 171, 193, and 211 Å from 14:00 to 19:00 UT. Totally, we collected about 1500 frames for each wavelength, with a temporal cadence of 12 s and a spatial resolution of 0.6 arcsec. We extracted a subfield of 1000 × 1000 pixels, which represents the region of interest. We increased the signal-to-noise ratio of the images by constructing a running mean datacube, where each frame is the sum of five consecutive frames corresponding to a time interval of 1 min: this allows improving the quality of the images and keeping the original temporal cadence. We took a slit at the apex of the loop, vertically and horizontally oriented (Fig. 4). Since the vertical slit offers the best projection in the SDO/AIA FOV, we focus our analysis on it. Starting from the vertical slit approximately located at the loop top, we built time-distance (TD) maps to depict transverse displacements.

3. Time-distance map analysis

To highlight the oscillatory patterns, we processed the TD maps by a "Laplacian" filter. The original TD maps were convolved with a kernel that defines the uni-dimensional Laplacian operator:

$$\hat{L} = \begin{pmatrix} 0 & -1 & 0 \\ 0 & 2 & 0 \\ 0 & -1 & 0 \end{pmatrix}. \quad (1)$$

The Laplacian operator defined in (1) is simply the second derivative along the vertical direction in the TD maps (hence the distance) and allows boundaries of the loop to be highlighted and the time dimension preserved. The result of the convolution operation between the TD map and the kernel is smoothed further with a Gaussian operator with a typical sigma of 1.5, in order to remove noise.

3.1. 171 Å

The filtered TD maps are given in Fig. 5 for 171, 193, and 211 Å. Bright patterns are clearly visible and outline the presence of close strands in the full loop structure, which are separated from

[1] The code is provided at http://www.astro.gla.ac.uk/~iain/demreg/

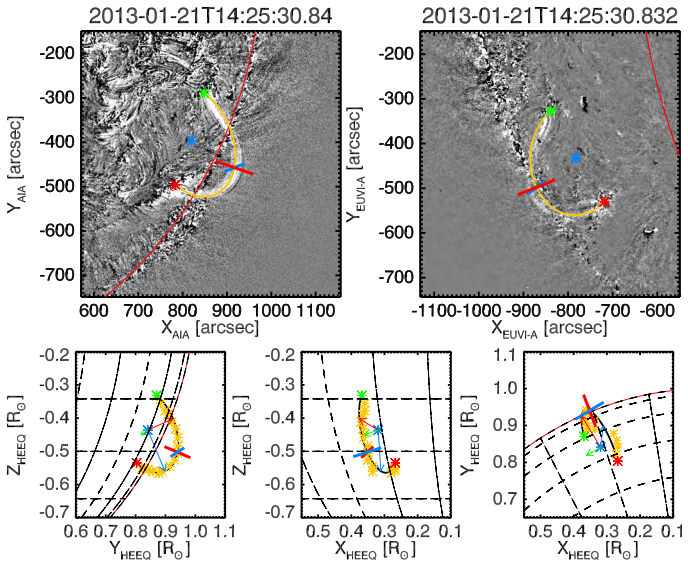

Fig. 4. *Top*: geometry reconstruction of the loop in 3D (yellow line) using difference images of SDO/AIA 193 (*top left*) and STEREO/EUVI-A 195 (*top right*) views. The northern loop footpoint is in green, whilst the southern one is in red, in blue the loop centre. The vertical (red) and horizontal (blue) slit is over-plotted. *Bottom*: projections of the loop in different orientations of the Heliocentric Earth EQuatorial (HEEQ) coordinate system. Distance are expressed in solar radii ($R_\odot$) units. The 3D data points are plotted as yellow points and fitted by the black line. The green, red and blue arrows mark respectively the normal plane, the minor and major radius of the loop. The red and blue lines at the loop apex locate the vertical and horizontal slits.

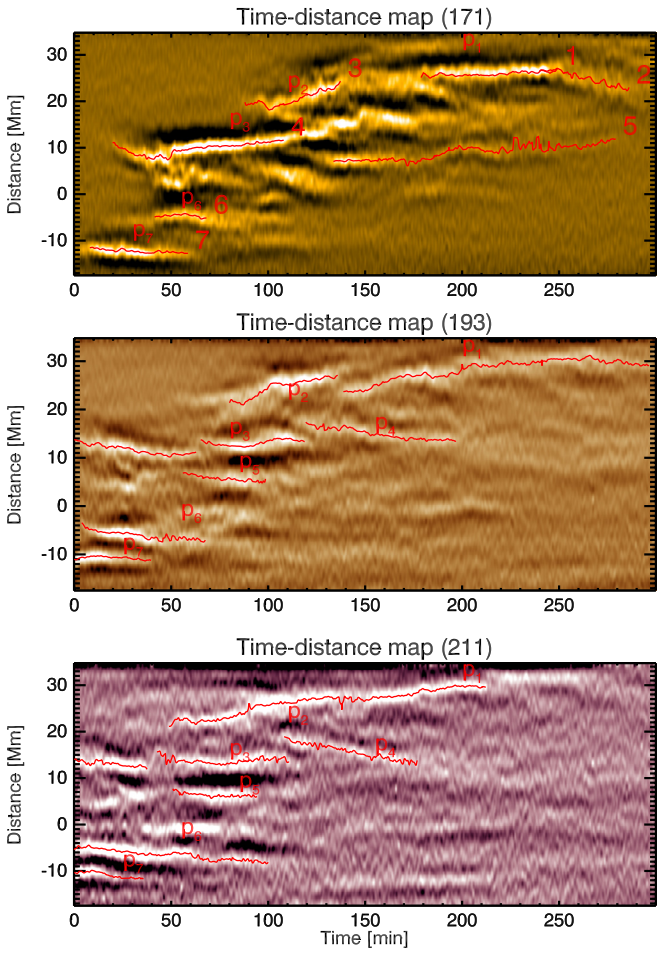

Fig. 5. Filtered TD maps at 171 (*top*), 193 (*middle*), and 211 Å (*bottom*). Oscillatory patterns obtained with an automatic Gaussian fitting are marked in red. The numbers shown are specifically related to the oscillatory patterns detected at 171 Å. The series of labels "p" refers to some segments of the patterns extracted and compared between 171, 193, and 211 Å, which are simultaneous and apparently from the same locations.

each other by less than 10 Mm. We automatically track the position of the bright patterns in TD maps by fitting the intensity of each vertical slice with a Gaussian function, where the maximum of the Gaussian locates the centre of the loop. Thus, time series of the loop displacements are obtained, and are over-plotted in red on the TD maps for the three wavelengths in Fig. 5.

The time series obtained from the 171 Å TD map are shown in the left-hand column of Fig. 6. To remove the global trend of the time series (that can be due to long-period local variations or also the solar rotation) and highlight oscillations, we fit them with one or more low-degree polynomial functions (green lines). The "de-trended" time series are plotted in the right-hand column of Fig. 5. The oscillations are depicted well, but show relevant variations both in amplitude and period. The oscillations seems to not be stationary. This can be proved by adapting some sine curves with specific period and amplitude just by an "eye estimation" of the oscillations (colour lines in left column plots). The agreement between data and empirical sine curves is kept only at some time intervals, for a few cycles of the oscillation. In different time intervals it is therefore necessary to use a sine curve with different parameters. This indicates that some external driver influences the loop oscillations, causing "intermittent" variation in amplitude and period. The values of the parameters of the sine curves are given in Table 1.

The extracted oscillations exhibit amplitudes close to the spatial resolution of the AIA pixel (i.e. ~0.435 Mm) ranging in values around 0.3–0.6 Mm, and some values lower than 0.2 Mm. The reason for the sub-resolution estimation of the oscillation amplitude is the Gaussian fitting method, as pointed out also in Morton & McLaughlin (2013) using AIA and the High Resolution Coronal Imager (HI-C) data.

3.2. Wavelet analysis

Since the observed transverse displacements of the loop are irregular in time, a more quantitative analysis can be done using the wavelet transform, which is often used in the analyses of time series with non-stationary power at different frequencies (Torrence & Compo 1998). Figure 7 gives the global and time wavelet spectra of the detrended time series shown in Fig. 6 (right). The wavelet spectra are obtained by considering the second derivative of a Gaussian (i.e. the Mexican hat) as the mother wavelet, and the smallest scale of size 0.4 min (24 s). The global spectra reveal the presence of broad peaks and in some case of distinct peaks, which confirm the irregular oscillations in the time series. The majority of the 95% confidence levels falls in the region that is not affected by the cone of influence (cross-hatched lines). The periods range from 4 to 16 min.

3.3. Comparison of the 171, 193, and 211 Å oscillatory patterns

A comparison of the oscillatory patterns seen at the different wavelengths can provide additional information on the dynamics of the loop. In Fig. 8 we plot a sequence of the oscillatory

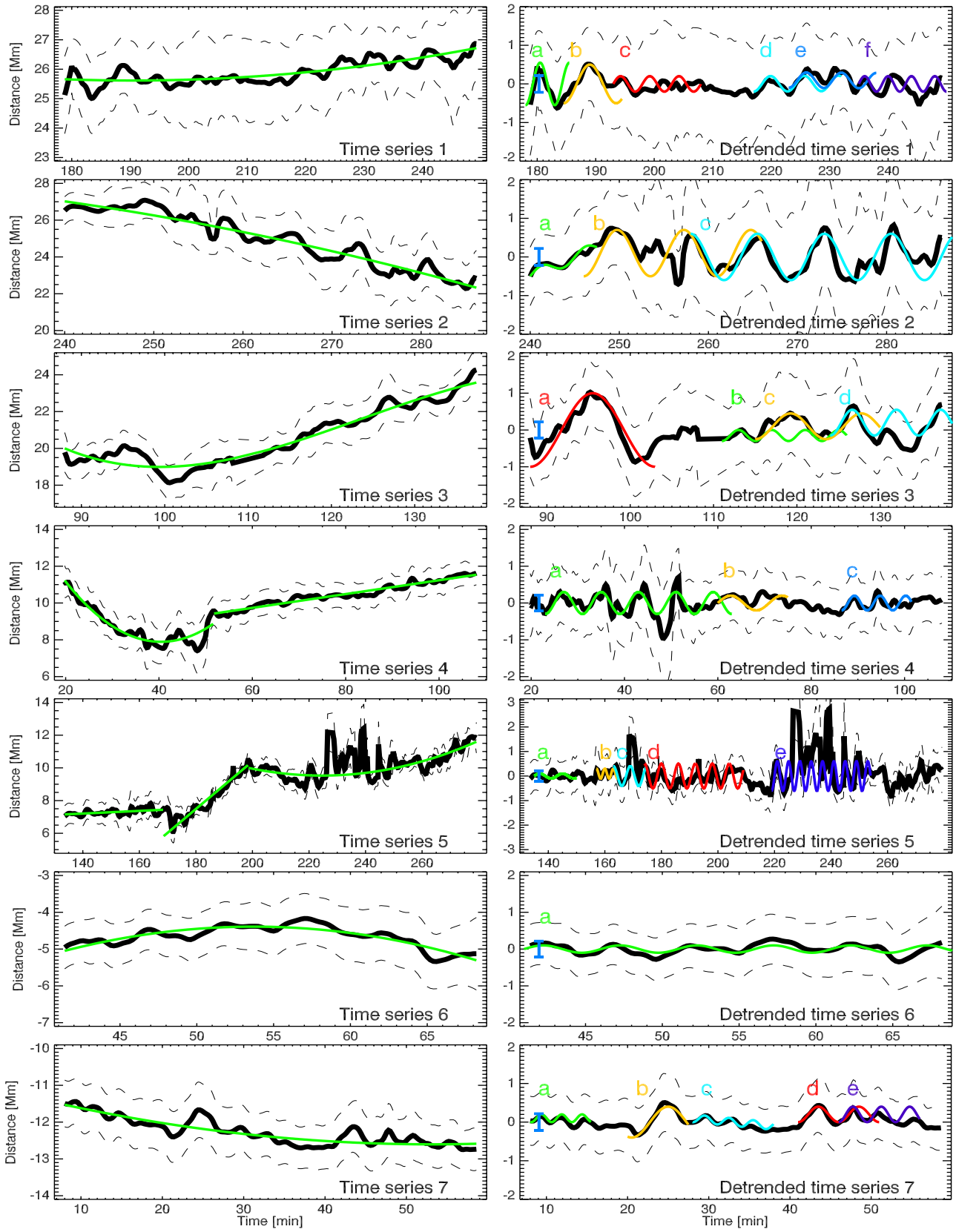

Fig. 6. Time series of the loop displacements extracted by a Gaussian fitting from the TD map at 171 Å of Fig. 5. The original time series are shown on the left. The dashed lines trace the loop boundaries and are estimated from the σ of the Gaussian fitting. The overall series are fitted with one or more low-degree polynomial functions (i.e. linear, quadratic, etc.) in order to determine their global trend, which has been removed in the *right plots*. A blue error bar in the *right column* of plots is shown in order to compare the amplitude of oscillations with the AIA spatial resolution (~0.4 Mm).

Table 1. Parameters of the "eye" fittings of Fig. 6.

N_{oscill}	t_0 [min]	y_0 [Mm]	ξ [Mm]	P [min]	ϕ [deg]
Oscill (1)					
a	178.0	0.0	0.55	5.0	–180
b	184.5	0.0	0.50	9.0	–180
c	193.0	0.0	0.20	5.0	–90
d	217.0	0.0	0.20	5.8	–180
e	223.0	0.1	0.20	6.0	–180
f	235.0	0.0	0.20	4.0	–90
Oscill (2)					
a	240.0	–0.5	0.15	5.0	–90
b	246.0	0.1	0.60	7.5	–180
c	258.0	0.0	0.60	7.5	0
Oscill (3)					
a	88.0	0.0	1.00	15.0	–180
b	111.0	–0.15	0.15	4.0	–180
c	115.0	0.1	0.35	8.5	–180
d	124.0	0.2	0.35	5.3	–180
Oscill (4)					
a	23.0	0.0	0.30	8.0	–180
b	60.0	0.0	0.20	11.0	–90
c	86.5	0.0	0.20	5.5	–180
Oscill (5)					
a	135.0	0.0	0.10	8.0	–90
b	157.0	0.1	0.20	3.0	0
c	163.0	0.0	0.40	6.0	0
d	174.0	0.0	0.50	6.0	0
e	219.0	0.0	0.60	4.0	–180
Oscill (6)					
a	41.0	0.0	0.10	5.0	–90
Oscill (7)					
a	8.0	0.1	0.10	2.5	–200
b	20.0	0.0	0.40	9.0	–200
c	28.0	0.1	0.10	3.0	–180
d	41.0	0.2	0.20	5.0	–180
e	46.0	0.2	0.20	3.5	–180

Notes. Some segments of the oscillations are empirically fitted with the sinusoidal function $y = y_0 + \xi \cos(2\pi(t - t_0)/P + \phi)$, with y_0 the offset along the distance, t_0 the initial time, ξ, P, and ϕ the amplitude, period, and phase of the oscillation, respectively. The related fittings are overlaid with different colours and labels (indicated in the first column) in Fig. 6.

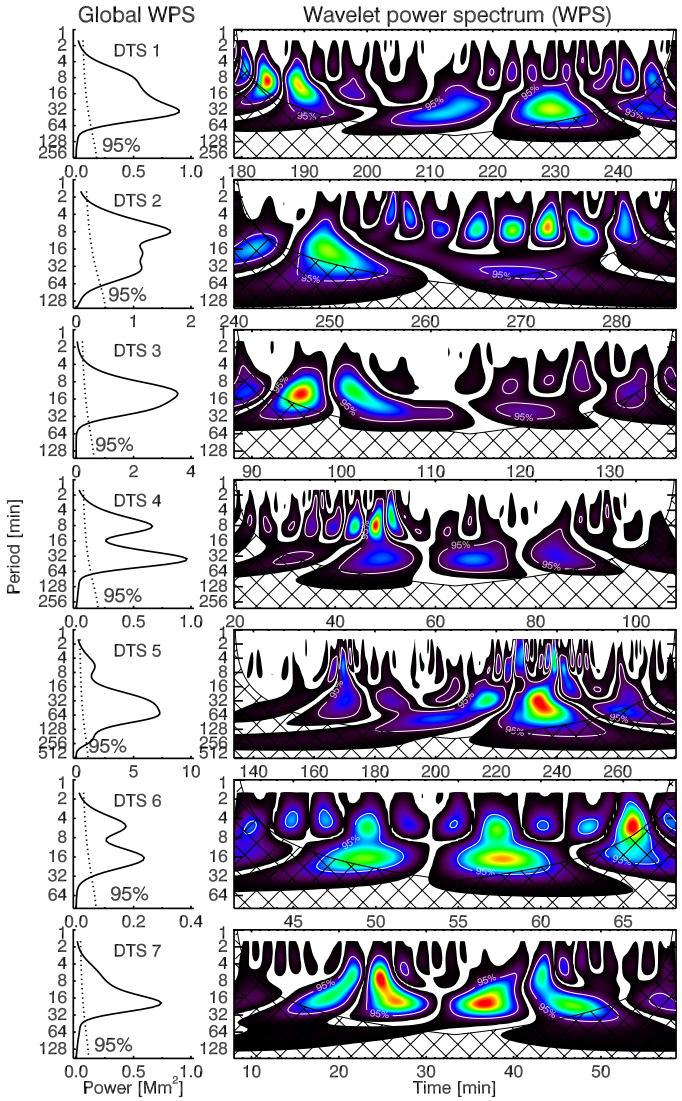

Fig. 7. Global (*left*) and time (*right*) wavelet power spectra of the detrended time series (DTS) shown in Fig. 6.

patterns seen at 171, 193, and 211 Å, which share almost the same spatial location. The left-hand column shows the oscillations as obtained from the TD maps: these are independently detrended with some polynomial functions and plotted in the right-hand column of Fig. 8. Subtracting different polynomials from each related time series should not introduce a major difference in the oscillations, since their time scale is much longer than the period of the oscillations. On the other hand, from the original time series, it is possible to notice that simultaneous oscillatory patterns, except for cases (p_{4-5}) at 193 and 211 Å, do not share the same location and do not overlap in the TD maps. This indicates that distinct strands, possibly under different physical conditions of temperature and density, do not contribute in the same way to each AIA filter. Moreover, the transverse displacements are not generally in phase, and because they are non-stationary displacements, they seem to respond differently to a stochastic driver.

4. Discussion and conclusions

In this work we analysed the transverse oscillations of a coronal loop in a quiet-Sun region close to the solar limb, as observed from SDO/AIA, in order to study and provide new highlights on the decay-less kink oscillation observed from Wang et al. (2012), Nisticò et al. (2013a), and Anfinogentov et al. (2013). The analysed loop was rather peculiar, because it was isolated well from other loops, not associated with a specific active region, and was visible simultaneously in different EUV wavelengths. Our findings can be summarised as follows.

1. The loop geometry was reconstructed in 3D from SDO/AIA 193 and STEREO/EUVI-A 195 views. We found that the loop can be modelled by an elliptical shape with a moderate eccentricity. The major axis is just 1.27 times larger than the minor one, so that the loop is almost circular. The plane of the loop is almost perpendicular to the solar surface, and it has a large azimuthal angle. The inspection of the AIA frames at several filters shows that the loop is possibly constituted of finer strands, probably at different physical conditions of density and temperature, as shown in the temperature analysis.
2. A TD map constructed from a slit located almost at the apex of the loop in the vertical (to the solar surface) direction shows the presence of small-amplitude kink oscillations,

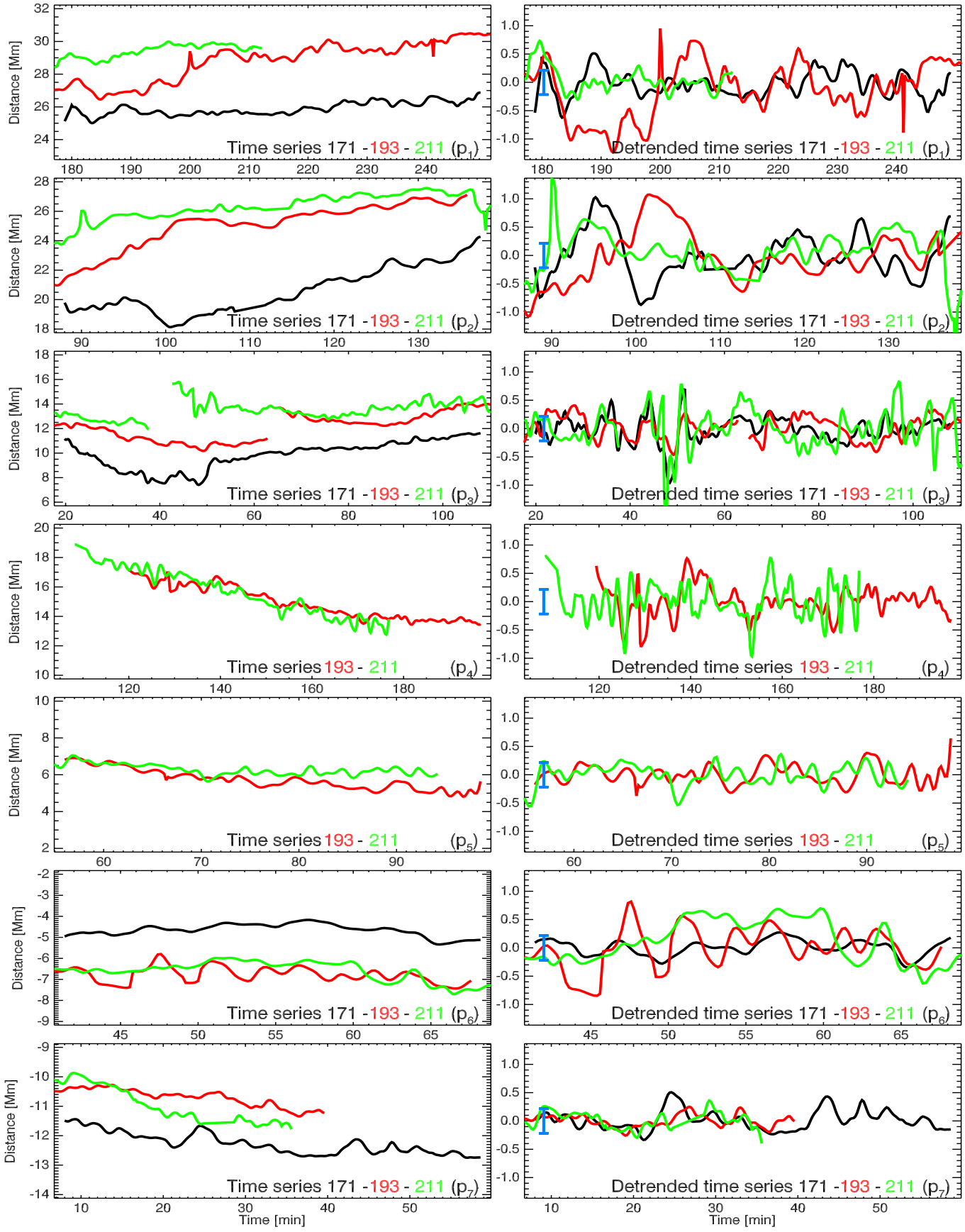

Fig. 8. Oscillatory patterns for the 171 (black), 193 (red), and 211 Å (green) obtained from the corresponding TD maps of Fig. 5. Each time series is independently detrended by some low-degree polynomial functions and shown in the *right column* of plots. The blue error bar shows the AIA pixel resolution equivalent to ~0.4 Mm.

comparable with the AIA spatial resolution. The oscillations, analysed at 171 Å, are automatically tracked with a Gaussian fitting technique and detrended with one or more background polynomial functions. They show some irregular variations in the period and amplitude. Only some certain time intervals can be "visually" fitted by a sinusoidal function with a constant period and amplitude. Wavelet power spectra show broad peaks in the range 4–16 min, with some drifts associated with the variations in the oscillation period and/or amplitude.

3. The comparison of oscillatory patterns simultaneously detected at 171, 193, and 211 Å show that they do not overlap in TD maps. This can be attributed to the possibility that they belong to specific strands that have different physical condition (temperature, density). Moreover the detrended oscillations detected in different bandpasses are all not in phase, having distinct periods and amplitudes.

The observed quasi-periodic transverse displacement of the multi-thermal loop makes its behaviour rather different than previously observed in coronal loops. Indeed, in contrast to the results obtained in the present study, the decay-less transverse oscillations previously detected in EUV loops were almost regular and monochromatic. The discrepancy can possibly be attributed to more effective damping of the oscillations in this loop. Consider kink oscillations of a coronal loop in terms of the empirical model suggested in Nisticò et al. (2013a). In this model the loop oscillations are described by a harmonic damped oscillator forced by an external driver. We assume that the driving force is random, representing, e.g., random granulation flows affecting the loop footpoints or random flows in the corona. If the damping term is not too strong, the oscillations have a frequency close to the natural frequency of the oscillator, i.e. the frequency of the global kink mode. But, if the damping term is very strong, the oscillation will follow the time pattern of the external driver. Perhaps what we see as the transverse displacements is therefore the induced solution – the loop displacements forced by the irregular driver. This interpretation is definitely speculative, and better understanding of this process requires a dedicated theoretical study, as well as an investigation into the techniques for extracting loop displacement measurements near the detection threshold.

The clearly different displacement patterns seen in the bandpasses that are associated with specific temperatures of the emitting plasma can possibly be attributed to the unresolved fine structuring. The threads of various temperature have similar geometrical properties, but may not have the same physical properties. Thus, they may be affected by the external driver differently, showing a different transverse displacement. The idea of the fine multi-thermal structuring of EUV coronal loops has already been employed in the previous multi-wavelength studies of MHD oscillations (e.g. King et al. 2003). We would like to stress that the nature of the external driver of the kink displacements is not known and should be subject to follow-up research.

This interpretation seems to be consistent with the previous assumption that kink oscillations in the multi-thermal loop are subject to more effective damping. Indeed, in the resonant absorption theory, the energy of collective kink oscillations goes to the unresolved torsional motions at a narrow resonant shell (Ruderman & Roberts 2002; Goossens et al. 2002, 2012). If the analysed loop is a bundle of multi-thermal threads, there can be many resonant layers in its cross-section. As a result, in this multi-thermal loop, the area of the resonant layers can be bigger than in usual mono-thermal loops, which would increase the efficiency of the resonant absorption of kink oscillations.

Acknowledgements. Data are courtesy of the SDO/AIA and STEREO/SECCHI teams. This work is supported by the Science and Technology Facilities Council (STFC), the Marie Curie PIRSES-GA-2011-295272 RadioSun project, the European Research Council under the SeismoSun Research Project No. 321141, the Russian Foundation of Basic Research under grant 13-02-00044, and the BK21 plus program through the National Research Foundation funded by the Ministry of Education of Korea.

Note added in proof. This study offers the possibility of proving results from numerical modelling of multi-stranded loops. An example is given by Luna et al. (2010), who show the existence of a broad spectrum of kink frequency, the absence of a collective mode of oscillations, and a dependence of the damping caused by the internal structure for different models of multi-stranded loops. A more detailed comparison between observations and theoretical models will be the subject of future works.

References

Anfinogentov, S., Nisticò, G., & Nakariakov, V. M. 2013, A&A, 560, A107
Arregui, I., Oliver, R., & Ballester, J. L. 2012, Liv. Rev. Sol. Phys., 9, 2
Aschwanden, M. J., Fletcher, L., Schrijver, C. J., & Alexander, D. 1999, ApJ, 520, 880
Cirtain, J. W., Golub, L., Lundquist, L., et al. 2007, Science, 318, 1580
Cooper, F. C., Nakariakov, V. M., & Tsiklauri, D. 2003, A&A, 397, 765
De Moortel, I., & Brady, C. S. 2007, ApJ, 664, 1210
Del Zanna, G. 2013, A&A, 558, A73
Edwin, P. M., & Roberts, B. 1983, Sol. Phys., 88, 179
Goossens, M., Andries, J., & Aschwanden, M. J. 2002, A&A, 394, L39
Goossens, M., Andries, J., Soler, R., et al. 2012, ApJ, 753, 111
Guarrasi, M., Reale, F., & Peres, G. 2010, ApJ, 719, 576
Hannah, I. G., & Kontar, E. P. 2012, A&A, 539, A146
King, D. B., Nakariakov, V. M., Deluca, E. E., Golub, L., & McClements, K. G. 2003, A&A, 404, L1
Lemen, J. R., Title, A. M., Akin, D. J., et al. 2012, Sol. Phys., 275, 17
Luna, M., Terradas, J., Oliver, R., & Ballester, J. L. 2010, ApJ, 716, 1371
Morton, R. J., & McLaughlin, J. A. 2013, A&A, 553, L10
Nakariakov, V. M., Ofman, L., Deluca, E. E., Roberts, B., & Davila, J. M. 1999, Science, 285, 862
Nisticò, G., Nakariakov, V. M., & Verwichte, E. 2013a, A&A, 552, A57
Nisticò, G., Verwichte, E., & Nakariakov, V. M. 2013b, Entropy, 15, 4520
Roberts, B. 1981, Sol. Phys., 69, 27
Roberts, B., Edwin, P. M., & Benz, A. O. 1984, ApJ, 279, 857
Ruderman, M. S., & Roberts, B. 2002, ApJ, 577, 475
Torrence, C., & Compo, G. P. 1998, Bull. Am. Meteorol. Soc., 79, 61
Vasheghani Farahani, S., Van Doorsselaere, T., Verwichte, E., & Nakariakov, V. M. 2009, A&A, 498, L29
Verwichte, E., Nakariakov, V. M., Ofman, L., & Deluca, E. E. 2004, Sol. Phys., 223, 77
Verwichte, E., Nakariakov, V. M., & Cooper, F. C. 2005, A&A, 430, L65
Wang, T., Ofman, L., Davila, J. M., & Su, Y. 2012, ApJ, 751, L27
Wang, T. J., & Solanki, S. K. 2004, A&A, 421, L33
White, R. S., Verwichte, E., & Foullon, C. 2012, A&A, 545, A129
Zajtsev, V. V., & Stepanov, A. V. 1975, Issledovaniia Geomagnetizmu Aeronomii i Fizike Solntsa, 37, 3